



Angle-independent structural colors of silicon

Højlund-Nielsen, Emil; Weirich, Johannes ; Nørregaard, Jesper; Garnæs, Jørgen; Mortensen, N. Asger; Kristensen, Anders

Published in:
Journal of Nanophotonics

Link to article, DOI:
[10.1117/1.JNP.8.083988](https://doi.org/10.1117/1.JNP.8.083988)

Publication date:
2014

Document Version
Publisher's PDF, also known as Version of record

[Link back to DTU Orbit](#)

Citation (APA):
Højlund-Nielsen, E., Weirich, J., Nørregaard, J., Garnæs, J., Mortensen, N. A., & Kristensen, A. (2014). Angle-independent structural colors of silicon. *Journal of Nanophotonics*, 8(1), 083988.
<https://doi.org/10.1117/1.JNP.8.083988>

General rights

Copyright and moral rights for the publications made accessible in the public portal are retained by the authors and/or other copyright owners and it is a condition of accessing publications that users recognise and abide by the legal requirements associated with these rights.

- Users may download and print one copy of any publication from the public portal for the purpose of private study or research.
- You may not further distribute the material or use it for any profit-making activity or commercial gain
- You may freely distribute the URL identifying the publication in the public portal

If you believe that this document breaches copyright please contact us providing details, and we will remove access to the work immediately and investigate your claim.

Journal of Nanophotonics

SPIDigitalLibrary.org/jnp

Angle-independent structural colors of silicon

Emil Højlund-Nielsen
Johannes Weirich
Jesper Nørregaard
Joergen Garnaes
N. Asger Mortensen
Anders Kristensen



SPIE

Angle-independent structural colors of silicon

Emil Højlund-Nielsen,^a Johannes Weirich,^b Jesper Nørregaard,^c
Joergen Garnaes,^b N. Asger Mortensen,^d and Anders Kristensen^{a,*}

^aTechnical University of Denmark, DTU Nanotech, Ørstedes Plads, Building 345E,
DK-2800 Kgs. Lyngby, Denmark

^bDFM A/S, Matematiktorvet 307, DK-2800 Kgs. Lyngby, Denmark

^cNIL Technology ApS, Diplomvej 381, DK-2800 Kgs. Lyngby, Denmark

^dTechnical University of Denmark, DTU Fotonik, Ørstedes Plads, Building 343,
DK-2800 Kgs. Lyngby, Denmark

Abstract. Structural colors are optical phenomena of physical origin, where microscale and nanoscale structures determine the reflected spectrum of light. Artificial structural colors have been realized within recent years. However, multilayer structures require substantial fabrication. Instead we considered one-layer surface textures of silicon. We explored four patterns of square structures in a square lattice with periods of 500, 400, 300, and 200 nm. The reflectivity and daylight-colors were measured and compared with simulations based on rigorously coupled-wave analysis with excellent agreement. Based on the 200-nm periodic pattern, it was found that angle-independent specular colors up to 60 deg of incidence may be provided. The underlying mechanisms include (1) the suppression of diffraction and (2) a strong coupling of light to localized surface states. The strong coupling yields absorption anomalies in the visual spectrum, causing robust colors to be defined for a large angular interval. The result is a manifestation of a uniformly defined color, similar to pigment-based colors. These mechanisms hold potential for color engineering and can be used to explain and predict the structural-color appearance of silicon-based textures for a wide range of structural parameters. © 2014 Society of Photo-Optical Instrumentation Engineers (SPIE) [DOI: [10.1117/1.JNP.8.083988](https://doi.org/10.1117/1.JNP.8.083988)]

Keywords: structural color; diffraction gratings; silicon; rigorously coupled-wave analysis; viewing angles.

Paper 13135SS received Dec. 1, 2013; revised manuscript received Apr. 2, 2014; accepted for publication Apr. 2, 2014; published online May 13, 2014.

1 Introduction

Structural colors are optical phenomena of physical origin, where microscale and nanoscale structures determine the reflected spectrum of light, although an unambiguous definition has not been settled yet.¹ The mechanisms of structural colors are categorized into thin-film interference, multilayer interference, diffraction-grating optical effects, and photonic crystal effects.¹ Two examples of structural color are silicon nanowires on oxide thin-film creating color specific resonant scattering² and the Morpho butterfly reflecting omnidirectional blue light due to a multilayer topography.³ Artificial multilayer topographies require substantial fabrication. In this article, we investigate the structural color appearances from single-material one-layer surface textures, which in our view is better up-scalable compared to typical approaches for structural coloration. We consider silicon as a high-index model system for nanostructured dielectric surfaces suitable for polymer replication methods, such as imprinting/embossing and injection-molding. The reflectivity mode devices discussed allow for a number of applications, where surface decoration provides color effects, for example logos, text decoration, or line art. The reflectivity of daylight colors is measured and compared to rigorously coupled-wave analysis (RCWA) simulations, to identify different regimes and predict color appearance. Our study

*Address all correspondence to: Anders Kristensen, E-mail: anders.kristensen@nanotech.dtu.dk

0091-3286/2014/\$25.00 © 2014 SPIE

provides an engineering method to specify a physical surface grating texture that will yield a desired novel angle-independent structural color, quantified by color measurements.

The experimental work presented here is based on four samples, each of size of $1 \times 1 \text{ cm}^2$, of artificial nanostructures fabricated on a single wafer using electron beam lithography and dry etching. The patterns, characterized as diffraction gratings, consist of square structures in a square lattice with periods of 500, 400, 300, and 200 nm. Scanning electron microscope images of the four samples can be seen in Figs. 1(a)–1(d). The overall structures appear more rounded as the period decreases. The heights of the structures are measured by atomic force microscopy (not shown) to be around 180 nm. Figures 1(e)–1(h) show photographs without subsequent software adjustments of the wafer illustrating the angular dependence of the reflected light under daylight illumination from a window. In particular, Fig. 1(e) illustrates the near-normal incidence specular colors of the four samples. In Fig. 1(f), a photograph is seen, taken along the diagonal axis and $\sim 45^\circ$ deg normal to the surface. Here, significant shifts in color have occurred compared to normal incidence. In general, the samples display a rich variation of reflected specular and diffraction-based colors, except for the area with a 200-nm period that seems to retain a more homogeneous color.

2 Theory

For background, the reflectivity and transmission angular distribution of periodic structures are given by the well-known grating equation,⁴ which qualitatively describes the studied two-dimensional (2-D) system:

$$n_1 \sin \theta_m - n_1 \sin \theta_{\text{in}} = \frac{m\lambda}{\Lambda}, \quad (\text{reflec.orders}), \quad (1)$$

$$n_2 \sin \theta_m - n_1 \sin \theta_{\text{in}} = \frac{m\lambda}{\Lambda}, \quad (\text{trans.orders}), \quad (2)$$

where n_1 and n_2 are the refractive indices of the incident medium (air) and transmission medium (silicon), respectively, θ_{in} is the incident angle of the light, and θ_m is the angle of the m 'th order

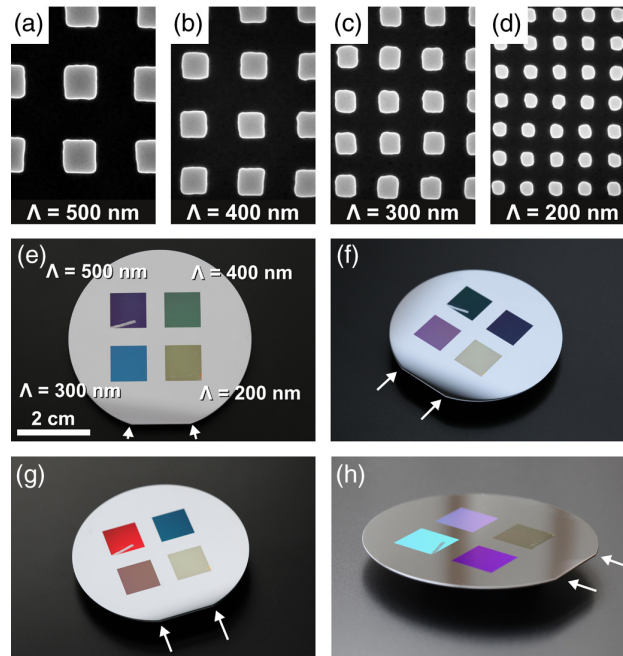


Fig. 1 Silicon structural colors. (a–d) Scanning electron microscope images $1.00 \mu\text{m}$ wide of the four periodic samples. (e–h) Photographs of the four samples from different angles. In (e), the camera is slightly tilted around 10 to 15 deg compared with normal incidence to avoid lens reflections.

reflectivity, both with respect to the surface normal, see Fig. 4(a). The transition from a non-diffractive to a diffractive reflective grating occurs at the corresponding Rayleigh wavelength;⁵ $\lambda_R(\theta_{in}) = \Lambda(\sin \theta_{in} + 1)$, where first-order ($m = 1$) emerges at glancing angle and the redistribution of energy results in an anomaly (rapid variation) in the specular reflectivity. In addition, a resonance type linked to leaky surface modes exists.⁶

In order to study these surface modes, finite element method frequency simulations are performed for the corresponding one-dimensional (1-D) grating in order to investigate near-field properties in side-view. A TM electromagnetic wave is normal incident on the 1-D grating, and a periodic phase-matched Floquet (Bloch) boundary condition is used. Results from a commercial available solver (Comsol 4.2, COMSOL Inc., Burlington, Massachusetts) can be seen in Fig. 2. It seems that a confinement of light, in the form of a high-electric field magnitude, occurs between the corners for wavelengths around 650 to 700 nm. The field is “short-circuited” between the vertical walls of the grating as described by Hessel and Oliner,⁶ to the extent that the corners almost appear to function as classical electromagnetic antennas. The field is concentrated in the air ($n = 1$). The boundary conditions force a discontinuity of the perpendicular electric field at the vertical grating walls due to the index contrast between the dielectric material and air, also utilized in the operation of slot-waveguides, as described by Almeida et al.⁷

In Fig. 3, the specular reflectivity calculated by RCWA for a 2-D grating is plotted as function of height and frequency. A period of 300 nm, a filling factor of 25%, a height of 180 nm, and a refractive index of 4.0 are used. The axes are normalized with respect to period exploiting the scale-invariance of Maxwell’s equations in the nondiffractive grating regime. In general, Fig. 3 holds great complexity. The features of reflectivity can be categorized into nonasymptotically features limited to certain heights and asymptotically features present at even large values of height. Regarding the nonasymptotically features, we find that they have similarities with the TM polarization features of the corresponding 1-D grating, similar to the results in Fig. 2. Regarding the asymptotically features, there exists no direct 1-D analogy. Instead, the authors find by band-structure calculations that these features to some extent can be understood as coupling the in-plane H-field to the corresponding 2-D photonic crystal modes at the Γ -point.

2.1 Color

The color of an object is the result of a complex interaction between the light source $S(\lambda)$ incident on the object, the reflectivity of the object $R(\lambda)$, and the observer. In the CIE (Commission Internationale de l’Éclairage) 1931 XYZ-model,⁸ colors can be defined on integral form:

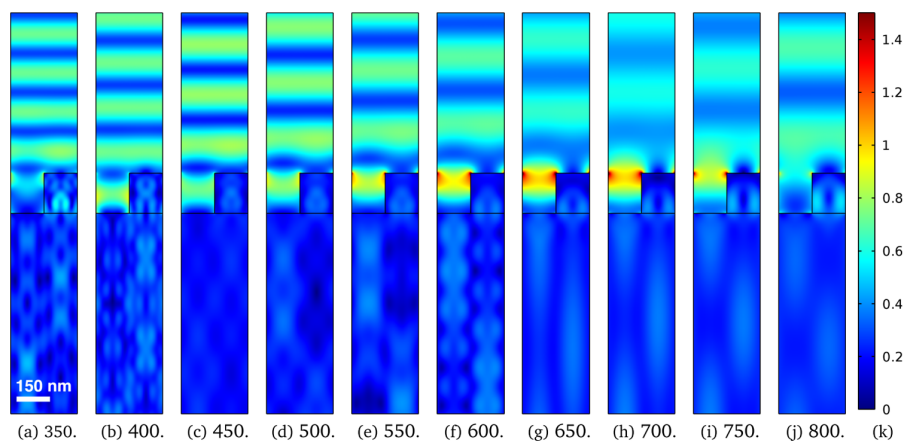


Fig. 2 Finite element method simulations of one-dimensional periodic grating and normal incidence TM electromagnetic wave. Contour plots of the electric field magnitudes with the air region to the left and the grating region to the right. Period 300 nm, width 150 nm, height 180 nm, and refractive index 4. (a–j) Total field magnitudes in millivolts per nanometers for an input power of 1 W. Numbers are wavelengths in nanometers. (k) Scale bar with a maximum of 1.5 (mV/nm).

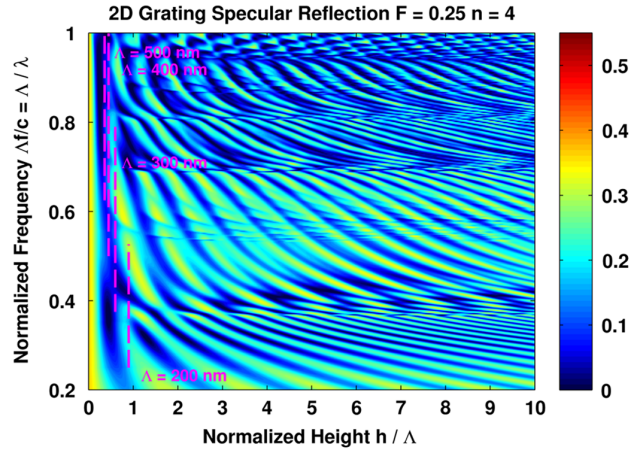


Fig. 3 Specular normal incidence reflectivity of a two-dimensional (2-D) square grating as function of normalized height and frequency simulated by rigorously coupled-wave analysis (RCWA) (350×400 points). Blue color indicates low reflectivity and red color indicates high reflectivity. A contour level of 0.3 corresponds to 30% of reflectivity. Refractive index 4. Dashed lines: 180-nm height.

$$\begin{bmatrix} X \\ Y \\ Z \end{bmatrix} \equiv C^{-1} \int_0^\infty S(\lambda) R(\lambda) \begin{bmatrix} \bar{x}_{\text{obs}}(\lambda) \\ \bar{y}_{\text{obs}}(\lambda) \\ \bar{z}_{\text{obs}}(\lambda) \end{bmatrix} d\lambda, \quad (3)$$

with normalization $C \equiv \int_0^\infty S(\lambda) \bar{y}_{\text{obs}}(\lambda) d\lambda$. Furthermore, we may define the chromaticity coordinates, independent of brightness $x \equiv X/(X + Y + Z)$, $y \equiv Y/(X + Y + Z)$. The parameters $(\bar{x}_{\text{obs}}, \bar{y}_{\text{obs}}, \bar{z}_{\text{obs}})$ describe the spectral sensitivity of the observer. Here, we use the 1978 Judd Vos correction⁹ of the CIE 1931 2° observer⁸ and the ISO/CIE standard illuminant D65.¹⁰ In order to accurately present color values, a conversion between the device-independent CIE-XYZ model and device-dependent outputs on a display (RGB) or paper (CMYK) is needed. Here, we adopt the sRGB conversion for display.¹¹ The grating scattering properties based on tabulated optical properties of silicon¹² are studied by RCWA,¹³ using a commercial solver (GD-Calc, KJ Innovation, Santa Clara, California).

The influence of specular and diffusive reflections on color perception under different light conditions has been discussed for a long time.^{14–18} In this letter, we focus on specular color effects. Conventionally, in color analysis, the specular part is often subtracted to give a more accurate description of color. However, in the case where the specular reflection provides a constant distinct output spectrum for a wide range of angles, the manifestation can be a more homogeneous color perception, if the illumination instead contains a diffusive component. The concept is justified by the photographs of Area 4 in Fig. 1.

3 Experimental Results

Reflection measurements are performed for TE/TM (not shown), and unpolarized light, using a xenon lamp (HPX-2000), two rotational stages, and a spectrometer (Jaz, Ocean Optics, Dunedin, Florida). The broad-spectrum white light from the xenon lamp is coupled via a multimode fiber to illuminate the sample at an angle of incidence θ_{in} . The reflected light is collected at an observer angle θ_{obs} , by the end of a multimode fiber and led into the spectrometer. With the definitions in Fig. 4(a), specular reflectivity is given by $\theta_{\text{obs}} = 2\theta_{\text{in}}$. The measurements are performed for $\phi_{\text{in}} = \{0^\circ, 45^\circ\}$, which is the maximum disparity for a symmetrical quadratic pattern. The absolute reflectivity is calculated using a reference measurement before and after each measurement.

The most important experimental results are plotted in Fig. 4. In Fig. 4(b), the measured specular reflectivity of the sample with a period of 300 nm can be seen as function of wavelength and angle of incidence for $\phi_{\text{in}} = \{0^\circ, 45^\circ\}$. The near-normal incidence measurements

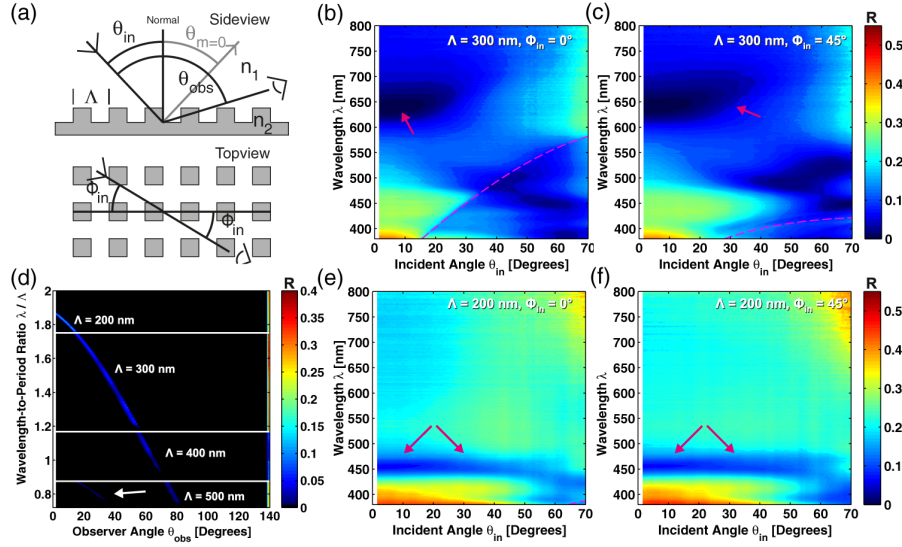


Fig. 4 Reflection measurements. (a) Sketch of measurement setup. (b) and (c) Specular reflectivity for the 300-nm period sample from 0% to 55% as function of incidence angle and wavelength for $\phi_{in} = \{0 \text{ deg}, 45 \text{ deg}\}$. Dashed lines mark Rayleigh line, arrows mark anomaly. (d) Measured reflectivity from 0% to 40% for a constant incidence angle of 70 deg as function of observer angle and normalized wavelength of the four samples. Arrow marks second order. (e) and (f) Specular reflectivity for the 200-nm period sample from 0% to 55% as function of incidence angle and wavelength for $\phi_{in} = \{0 \text{ deg}, 45 \text{ deg}\}$. Dashed line in bottom right corner marks Rayleigh line, arrows mark anomaly. Resolution $\Delta\theta = 0.5 \text{ deg}$.

show a distinctive minimum at a wavelength of 640 nm, corresponding to a normalized frequency of $\Lambda/\lambda = 0.47$ and a normalized height of $h/\Lambda = 0.58$, which by the simulations displayed in Figs. 2 and 3 are found to indicate a resonance anomaly behavior with strong coupling to a leaky surface wave.⁶ The relatively high reflectivity for short wavelengths can be explained as a combination of a rapidly increasing refractive index of silicon for short wavelengths and the absence of anomalies for the particular parameters.¹⁹ Regarding angular dependence, the distinctive line of low reflectivity in Fig. 4(b) can be identified as the “Rayleigh line,” meaning that diffraction in the visual spectrum does not occur until 15-deg incident angle. Thereby, the measurements for a period of 300 nm capture the transition from the nondiffractive regime of exclusive specular reflectivity at normal incidence to the diffraction regime for larger incidence angles, also supported by the tendency of low reflectivity for wavelengths shorter than the Rayleigh line due to the appearance of higher reflectivity orders.

In Figs. 4(e)–4(f), the measured specular reflectivity of the sample with a period of 200 nm can be seen as function of wavelength and angle of incidence, performed for $\phi_{in} = \{0 \text{ deg}, 45 \text{ deg}\}$ in Fig. 4(a). A high near-normal incidence reflectivity for short wavelengths below 400 nm is seen together with a sharp feature of low reflectivity around 455 nm. The minimum corresponds to a normalized frequency of 0.44. Assuming that a filling factor of 25% and a refractive index of 4 is reasonable here, we read of Fig. 3 a minimum at 0.44 for a normalized height of $171 \text{ nm}/200 \text{ nm} = 0.86$. Compared to the other three samples, the high-reflection wavelengths above 455 nm can be understood by the movement to the right in Fig. 3 away from the first air resonance and by the “scaling” of the normalized frequency, where the interval given by the visual spectrum is less broad compared with the 300-nm period. The scaling of the normalized frequency indicates the trade-off for small periods between avoiding diffraction for large incident angles and the normal incidence anomaly density, as the number of anomalies decreases for lower frequencies. Furthermore, it is clear that the anomalies do not shift wavelength for a large angle interval, indicating the coupling to an intrinsic localized surface state, and not a thin-film reflection from an effective medium, where a shift in minimum wavelength for larger incidence angles would have been observed. Regarding diffraction described by Eqs. (1) and (2), this does not occur in reflection mode until 64 deg for 200-nm periodic

structures in the visual spectrum ($\lambda_R = 380$ nm). Therefore, the structural colors originating from 200-nm periodic structures only exhibit minor angular dependence up to 60 deg incidence in all azimuthal directions, as seen in Fig. 4, due to the suppression of diffraction and the substituted strong coupling of light to localized surface states.

Besides measuring the specular reflectivity, one measurement for each sample is conducted as a sanity check, where the incidence angle is held constant at an angle of $\theta_{in} = 70$ deg along the horizontal direction, while the observer angle is varied. The measured TM reflectivity can be seen in Fig. 4(d), confirming that the angle distribution of the reflectivity is due to diffraction described by Eq. (1), supporting that diffraction must be suppressed before coupling to surface states can be utilized for wide angular illumination.

4 Discussion

The calculated sRGB color values of the measurements and corresponding simulations are plotted and displayed as function of incident angle in Figs. 5(a) and 5(b) for the horizontal ($\phi_{in} = 0$ deg) and diagonal directions ($\phi_{in} = 45$ deg). In terms of color, the sample with a period of 300 nm appears blue due to a low reflectivity of red light around the earlier mentioned minimum at 640 nm and high reflectivity around 400 nm. The shift to a brown/orange color at 30 deg incidence seen in Fig. 1(g) is due to the appearance of first-order diffraction cutting off the normal incidence features and the increase in Fresnel reflectivity for larger incidence angles.

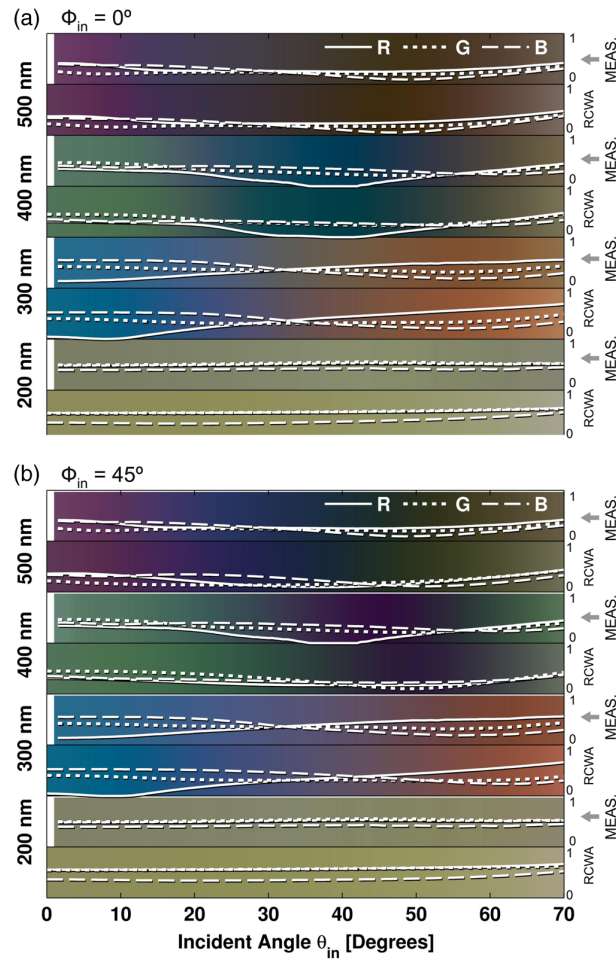


Fig. 5 Measured and RCWA-simulated silicon specular structural sRGB colors, scaled from 0 to 1, of the four samples as function of incident angle. (a) $\phi_{in} = 0$ deg and (b) $\phi_{in} = 45$ deg.

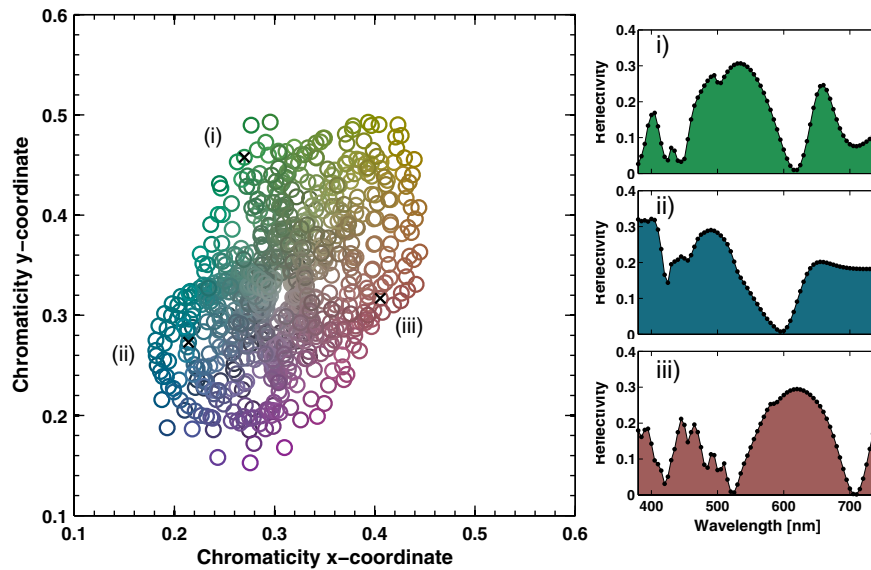


Fig. 6 Simulated silicon normal incidence specular colors by 2-D square gratings. (x, y) CIE chromaticity coordinates of the resulting spectra colored by the corresponding sRGB colors. Inset (i) Example of green color by parameters height 250 nm, period 240 nm, and filling factor 30%. Inset (ii) Example of blue color by parameters height 180 nm, period 210 nm, and filling factor 50%. Inset (iii) Example of red color by parameters height 300 nm, period 240 nm, and filling factor 48%.

The main differences between the horizontal and diagonal reflectivities, leading to shifts in color, can be understood by the shorter projected effective period Λ' seen by the diffracted light for the diagonal direction, ideally $\Lambda/\sqrt{2}$ for an incident angle of 90 deg. In general, the calculated colors in Fig. 5 are found by visual inspection to resemble daylight color accurately.

We may combine the colors portrayed here with the earlier measured diffraction results, by viewing a given grating sample under two incoherent light sources, such that the main specular reflectivity is observed using one source and a diffraction order is observed using the other source, similar to the red color seen in Fig. 1(g). As the diffraction order redirects light in the direction of the observer, the combination yields additive color mixing, in contrast to the specular absorptive colors. The implication, illustrated in Figs. 1(g) and 1(h), is the marvel of color effects taking place when the specular color appearances are accompanied by diffraction effects pointing to the difficulty of unambiguously defining structural colors.

Given the binary geometry used in this letter, what possible colors may be produced? In Fig. 6, an answer is given in the form of plotting the normalized chromaticity coordinates of normal incidence specular reflectivity simulations converted into a color via Eq. (3). Squared 2-D silicon gratings are modeled with parameters of 30- to 300-nm periods, structure heights of 120 to 300 nm, and filling factors between 10% and 90%. The color gamut seen in Fig. 6 indicates the possibilities of the technology. In general, it is found that colors become stronger for shorter periods below 240 nm.

One application for angular independent textures with periods in the 200 nm range is color reference cards used in the graphics industry. Today paper charts with pigments are used, which tend to fade after few years in service. The colors displayed in Fig. 6 can be fabricated in silicon with a high durability. With an appropriate coating applied to protect the nanostructures, the robustness and lifetime of the device may be significantly extended compared to current technology.

5 Conclusion

In conclusion, the structural color appearance of silicon diffraction gratings was examined based on four samples with periods of 500, 400, 300, and 200 nm. The reflectivity and

daylight-colors were measured and compared to simulations based on RCWA and CIE color theory. The method was used to predict the structural color appearance for a wide range of design parameters. Finally, nondiffractive angle-independent colors up to 60 deg of incidence may be provided by suppressing diffraction and instead couple to normal incidence absorption anomalies.

Acknowledgments

We acknowledge DTU colleagues T. Buss for experimental assistance and J. Scheel for photography. This work was supported by the Danish National Advanced Technology Foundation (Contract No.: 007-2010-2) and by the European Commission via the FP7 MMP Integrated project Plast4Future (NMP2-SE-2012-314345). Emil Højlund-Nielsen did the experimental work, the simulations, and prepared the manuscript. Johannes Weirch assisted the RCWA simulations and performed the data fitting, Jesper Nørregaard provided the sample and supervised, Joergen Garnaes did the AFM measurements. Finally, N. Asger Mortensen and Anders Kristensen supervised.

References

1. S. Kinoshita, S. Yoshioka, and J. Miyazaki, "Physics of structural colors," *Rep. Prog. Phys.* **71**(7), 076401 (2008), <http://dx.doi.org/10.1088/0034-4885/71/7/076401>.
2. L. Cao et al., "Tuning the color of silicon nanostructures," *Nano Lett.* **10**(7), 2649–2654 (2010), <http://dx.doi.org/10.1021/nl1013794>.
3. P. Vukusic and J. R. Sambles, "Photonic structures in biology," *Nature* **424**, 852–855 (2003), <http://dx.doi.org/10.1038/nature01941>.
4. D. H. Raguin and G. M. Morris, "Analysis of antireflection-structured surfaces with continuous one-dimensional surface profiles," *Appl. Opt.* **32**(14), 2582–2598 (1993), <http://dx.doi.org/10.1364/AO.32.002582>.
5. J. E. Stewart and W. S. Gallaway, "Diffraction anomalies in grating spectrophotometers," *Appl. Opt.* **1**(4), 421–430 (1962), <http://dx.doi.org/10.1364/AO.1.000421>.
6. A. Hessel and A. A. Oliner, "A new theory of wood anomalies on optical gratings," *Appl. Opt.* **4**(10), 1275–1297 (1965), <http://dx.doi.org/10.1364/AO.4.001275>.
7. V. R. Almeida et al., "Guiding and confining light in void nanostructure," *Opt. Lett.* **29**(11), 1209–1211 (2004), <http://dx.doi.org/10.1364/OL.29.001209>.
8. T. Smith and J. Guild, "The C.I.E., colorimetric standards and their use," *Trans. Opt. Soc.* **33**(3), 73–134 (1931), <http://dx.doi.org/10.1088/1475-4878/33/3/301>.
9. J. J. Vos, "Colorimetric and photometric properties of a 2 fundamental observer," *Color Res. Appl.* **3**(3), 125–128 (1978), [http://dx.doi.org/10.1002/\(ISSN\)1520-6378](http://dx.doi.org/10.1002/(ISSN)1520-6378).
10. D. B. Judd et al., "Spectral distribution of typical daylight as a function of correlated color temperature," *J. Opt. Soc. Am.* **54**(8), 1031–1040 (1964), <http://dx.doi.org/10.1364/JOSA.54.001031>.
11. M. Stokes et al., "A standard default color space for the Internet—sRGB <http://www.w3.org/Graphics/Color/sRGB.html> (checked 2013-04-20)" (1995).
12. M. A. Green and M. J. Keevers, "Optical properties of intrinsic silicon at 300 K," *Prog. Photovoltaics Res. Appl.* **3**(3), 189–192 (1995), [http://dx.doi.org/10.1002/\(ISSN\)1099-159X](http://dx.doi.org/10.1002/(ISSN)1099-159X).
13. M. N. Nevière and M. N. E. Popov, *Light Propagation in Periodic Media: Differential Theory and Design*, Optical Engineering Series, Marcel Dekker, Inc., New York (2003).
14. H.-C. Lee, "Method for computing the scene-illuminant chromaticity from specular highlights," *J. Opt. Soc. Am. A* **3**(10), 1694–1699 (1986), <http://dx.doi.org/10.1364/JOSAA.3.001694>.
15. R. Shapley, "Neural mechanisms for color perception in the primary visual cortex," *Curr. Opin. Neurobiol.* **12**(4), 426–432 (2002), [http://dx.doi.org/10.1016/S0959-4388\(02\)00349-5](http://dx.doi.org/10.1016/S0959-4388(02)00349-5).
16. J. N. Yang and L. T. Maloney, "Illuminant cues in surface color perception: tests of three candidate cues," *Vision Res.* **41**(20), 2581–2600 (2001), [http://dx.doi.org/10.1016/S0042-6989\(01\)00143-2](http://dx.doi.org/10.1016/S0042-6989(01)00143-2).

17. S. K. Nayar, X.-S. Fang, and T. Boulton, "Separation of reflection components using color and polarization," *Int. J. Comput. Vision* **21**(3), 163–186 (1997), <http://dx.doi.org/10.1023/A:1007937815113>.
18. S. Tominaga, "Surface identification using the dichromatic reflection model," *IEEE Trans. Pattern Anal. Mach. Intell.* **13**(7), 658–670 (1991), <http://dx.doi.org/10.1109/34.85656>.
19. G. Bao, D. C. Dobson, and K. Ramdani, "A constraint on the maximum reflectance of rapidly oscillating dielectric gratings," *SIAM J. Control Optim.* **40**(6), 1858–1866 (2002), <http://dx.doi.org/10.1137/S036301290037435X>.

Emil Højlund-Nielsen is a PhD student within structural colors at the Technical University of Denmark, where he also received his MSc degree within physics and nanotechnology in 2012. He develops nanoscale designs for structural coloration. He is experienced within teaching, cleanroom fabrication, numerical modeling, and optical characterization of micro- and nanosystems.

Johannes Weirich is a staff scientist at DFM A/S. He received his PhD degree within optics in liquid crystal photonic bandgap fiber devices from Technical University of Denmark in 2010. He does development and application of numerical and experimental optical methods. More specifically, he has experience in optics (fiber optics, lasers, optical micro- and nanostructures), modeling and numerical methods (finite element, finite difference), and design and implementation of simulation tools (based on Python, C/C++, and Fortran).

Jesper Nørregaard is R&D manager at NIL Technology ApS. He has many years of experience with high-tech startups and large experience with the development of business models and maturation of products. He received his PhD in physics from University of Copenhagen in 1989 and has been working mainly in private companies as a manager of R&D or manufacturing of semiconductors or photonic devices. He also serves as a board member in smaller companies and holds several patents.

Joergen Garnæs is staff scientist at DFM A/S. He received his PhD in 1991 from Laboratory of Applied Physics, Technical University of Denmark. He does research within surface metrology and scanning probe microscopy investigations of industrial and applied surfaces. He is coauthor of more than 50 publications in international refereed scientific journals, two of which have been in *Nature* and one in *Science*.

N. Asger Mortensen is professor at the Technical University of Denmark (DTU) from which he also received the MSc, PhD, and Dr. Techn. degrees in 1998, 2001, and 2006, respectively. His research interest and experience are centered on theoretical and computational physics, including condensed matter theory, photonics, optofluidics, plasmonics, and metamaterials. He is the author of more than 160 journal papers and has written three book chapters.

Anders Kristensen is professor in miniaturized sensor and actuator technology at the Technical University of Denmark. He received his MSc and PhD degrees in physics from the University of Copenhagen in 1991 and 1984, respectively. He is the author of more than 120 peer-reviewed journal papers and has written three book chapters. His current research interests include optofluidics, nanofluidics, nanoimprint lithography, and structural colors. He is the coordinator of several international research projects.